Progress In Electromagnetics Research, Vol. 160, 41–50, 2017

Surface Impedance Synthesis Using Parallel Planar Electric Metasurfaces

Bo O. Zhu*

Abstract—Metasurfaces, due to its designable surface electric and magnetic impedances, have largely enhanced electromagnetic wave manipulation techniques. The conventional approach to realize the surface magnetic impedance requires non-planar structures, such as metallic loops, which is not easy to fabricate, especially at optical frequencies. In this work, we theoretically and rigorously prove that effective surface magnetic and electric impedances can be obtained using parallel electric metasurfaces. A synthesis method is presented which allows independent designs of surface electric and magnetic impedances. Finally, a polarization converter with high energy efficiency is designed using the proposed impedance synthesis method for verification. The proposed synthesis method is favorable for reducing fabrication complexities.

1. INTRODUCTION

The recently proposed metasurface is a two-dimensional array of subwavelength scatterers [1–9]. It is a promising way to manipulate electromagnetic (EM) wave propagation because of the designable feature of its surface impedance, which uniquely determines the EM field behavior. Many novel metasurface devices have been proposed so far, such as planar chiral plates [10], holography [11], spin-controlled photonics [12], wave orbital angular momentum manipulations [13–16], polarization converters and quarter-wave plates [17, 18], flat lens and focusing [19–22], and Huygens metasurfaces [23, 24].

The surface impedance of metasurfaces comes from the shapes and periodicity of the subwavelength scatterers of metasurfaces. Because of the subwavelength feature of the periodic scatterers, only the fundamental Floquet mode, that is just a plane wave, can propagate; whereas the high-order Floquet modes are evanescent along the propagation direction, and contribute to the surface impedance of a metasurface. The surface impedance of a metasurface can be categorized into electric type and magnetic type. Both of them are important and necessary to achieve full control on EM wave propagation [23, 24]. The electric surface impedance is usually implemented by ultra-thin metallic patterns [4, 14, 17, 18, 25–27], whereas the magnetic surface impedance is usually implemented by the metallic loops [7, 23, 24, 28].

Obviously, this type of magnetic surface impedance requires the non-planar fabrication process, which is usually difficult to be met, especially in optical regimes [29]. Of late, some planar metasurfaces have been proposed, which are suitable for microscopic fabrication so as to work at quite high frequencies [30–33]. In this article, we will theoretically and rigorously prove that the effective surface magnetic impedance can be achieved by employing parallel planar metasurfaces with only identical surface electric impedances. Moreover, deep physics insight from this analysis show that adding another electric metasurface at the middle between the original parallel metasurfaces can adjust the effective electric surface impedance with no influence on the effective magnetic surface impedance achieved originally. Directed by the theory, a linear to circular polarization converter with high energy efficiency is designed to demonstrate the effectiveness of this approach.

Received 19 June 2017, Accepted 7 October 2017, Scheduled 31 October 2017

* Corresponding author: Bo O. Zhu (bzhu@nju.edu.cn).
The author is with the School of Electronic Science and Engineering, Nanjing University, Nanjing 210023, China.

2. FUNDAMENTAL THEORY

Figure 1(a) shows two electric metasurfaces located at $z = \pm a/2$ respectively, which are illuminated by a normal incident plane EM wave. The surface electric current $\mathbf{J}^{\pm}$ is induced under the excitation, which can be further decomposed into the odd mode current $\mathbf{J}_o^{\pm}$ with $\mathbf{J}_o^{-} = -\mathbf{J}_o^{+}$, and the even mode current $\mathbf{J}_e^{\pm}$ with $\mathbf{J}_e^{-} = \mathbf{J}_e^{+}$, as illustrated in Figs. 1(b) and (c) respectively. The microscopic Maxwell equations for this case are

$$\nabla \times \mathbf{E} = -\frac{\partial \mathbf{B}}{\partial t}, \tag{1a}$$

$$\nabla \times \frac{\mathbf{B}}{\mu_0} = \frac{\partial (\epsilon_0 \mathbf{E})}{\partial t} + \mathbf{J}_o + \mathbf{J}_e. \tag{1b}$$

Since $\mathbf{J}_o$ is circulating and divergence free, it produces magnetic dipole polarization density $\mathbf{M}$ with the relation $\nabla \times \mathbf{M} = \mathbf{J}_o$. Inserting this relation into Eq. (1b) with some arrangement, we have

$$\nabla \times \left(\frac{\mathbf{B}}{\mu_0} - \mathbf{M} \right) = \frac{\partial \mathbf{D}}{\partial t} + \mathbf{J}_e \tag{2}$$

With the Definition $\mathbf{H} = \frac{\mathbf{B}}{\mu_0} - \mathbf{M}$, Eq. (1) becomes

$$\nabla \times \mathbf{E} = -\frac{\partial (\mu_0 \mathbf{H})}{\partial t} - \frac{\partial (\mu_0 \mathbf{M})}{\partial t}, \tag{3a}$$

$$\nabla \times \mathbf{H} = \frac{\partial (\epsilon_0 \mathbf{E})}{\partial t} + \mathbf{J}_e, \tag{3b}$$

indicating that the induced odd mode current $\mathbf{J}_o$ results in an equivalent magnetic polarization density $\partial(\mu_0 \mathbf{M})/\partial t$, which leads to the tangential electric field discontinuity and the effective surface magnetic impedance. The even mode current $\mathbf{J}_e$ is associated with the surface electric impedance.

2.1. Effective Surface Magnetic Impedance

It needs some calculation to establish the quantitative relation between the effective surface impedance and the constitutive parallel electric metasurfaces. Time factor $e^{j\omega t}$ is adopted and suppressed throughout below. Assuming a plane wave is incident from the left to the right, as shown in Fig. 1(a),

$$\mathbf{E}^i = E_x^i e^{-jkz} \hat{\mathbf{x}}, \tag{4a}$$

$$\mathbf{H}^i = H_y^i e^{-jkz} \hat{\mathbf{y}}. \tag{4b}$$

Using Faraday's law

$$\oint_L \mathbf{E}^i \cdot \mathbf{dl} = -j\omega\mu_0 \int_S \mathbf{H}^i \cdot \mathbf{ds}, \tag{5}$$

we have

$$E_x^{i-} \hat{\mathbf{x}} \cdot -\mathrm{d}l \hat{\mathbf{x}} + E_x^{i+} \hat{\mathbf{x}} \cdot \mathrm{d}l \hat{\mathbf{x}} = -j\omega\mu_0 \mathrm{d}l \int H_y^i e^{-jkz} \hat{\mathbf{y}} \cdot \mathrm{d}z \hat{\mathbf{y}}, \tag{6}$$

where $E_x^{i\pm}$ denotes the incident electric field complex amplitudes at $z = \pm a/2$ respectively. Eq. (6) can be rewritten with some simplification as

$$\Delta \mathbf{E}^i = (E_x^{i-} - E_x^{i+}) \hat{\mathbf{x}} \approx j\omega\mu_0 a H_y^i \hat{\mathbf{x}}, \tag{7}$$

where the first order approximation $e^{-jka} \approx 1 - jka$ is used when a is much smaller than wavelength [3–5]. This approximation, which is normally valid in metasurface designs, is used throughout this paper. The odd mode of the incident electric field acting on the metasurfaces at $z = \mp a/2$ are $\pm \Delta \mathbf{E}^i/2$ respectively, as illustrated in Fig. 1(b). Such an odd mode electric field excites an odd mode surface electric current $\mathbf{J}_o$ if the parallel electric metasurfaces are identical. For the non-identical case, chiral effect will occur, which is outside the scope of this paper. The scattering electric and magnetic fields due to $\mathbf{J}_o^{-}$ are $E_{ox}^{s-} e^{-jk(z+a/2)} \hat{\mathbf{x}}$ and $\frac{E_{ox}^{s-}}{\eta} e^{-jk(z+a/2)} \hat{\mathbf{y}}$ respectively for $z > -a/2$ region, and $E_{ox}^{s-} e^{jk(z+a/2)} \hat{\mathbf{x}}$ and

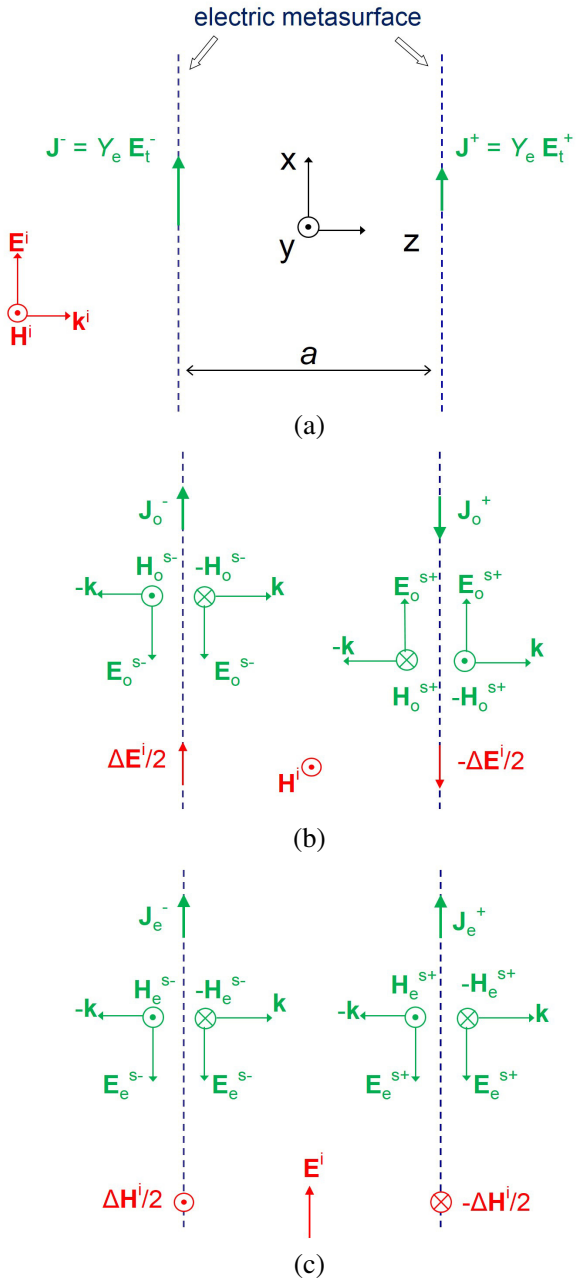

Figure 1. Working principle of the effective magnetic surface impedance produced by double-layer planar electric surface. Red color denotes the primary exciting fields, and green one denotes the responding induced current and scattered fields. The superscript '−/+' distinguish the field quantities on the left/right metasurface. (a) Two electric metasurfaces separated by distance a under the normal incidence. The exciting electric field can be decomposed into odd and even components, producing the odd and even surface currents, as shown in (b) and (c). (b) The incident magnetic field excites differential electric fields (odd mode) acting on the metasurfaces to produce the odd mode surface electric current. (c) The average incident electric field produces the even mode surface electric current on the metasurfaces.

$\frac{-E_{ox}^{s-}}{\eta}e^{jk(z+a/2)}\hat{\mathbf{y}}$ respectively for $z<-a/2$ region. Similarly, the scattering electric and magnetic fields due to $\mathbf{J}_o^+$ are $E_{ox}^{s+}e^{-jk(z-a/2)}\hat{\mathbf{x}}$ and $\frac{E_{ox}^{s+}}{\eta}e^{-jk(z-a/2)}\hat{\mathbf{y}}$ respectively for $z>a/2$ region, and $E_{ox}^{s+}e^{jk(z-a/2)}\hat{\mathbf{x}}$ and $\frac{-E_{ox}^{s+}}{\eta}e^{jk(z-a/2)}\hat{\mathbf{y}}$ respectively for $z<a/2$ region, where $E_{ox}^{s-}=-E_{ox}^{s+}$ since $\mathbf{J}_o^-=-\mathbf{J}_o^+$.

The total electric field acting on the metasurface at $z=-a/2$ is

$$\mathbf{E}_t^- = \left(\frac{1}{2}j\omega\mu_0 a H_y^i + E_{ox}^{s-} + E_{ox}^{s+}e^{-jka}\right)\hat{\mathbf{x}}, \tag{8}$$

which induces the surface electric current

$$\mathbf{J}_o^- = -2\frac{E_{ox}^{s-}}{\eta}\hat{\mathbf{x}}. \tag{9}$$

Applying the surface electric impedance definition $\mathbf{J}=Y_e\mathbf{E}$ to Eqs. (8) and (9), we can determine E_x^{s-} given the incident field H_y^i as

$$E_{ox}^{s-} = \frac{\frac{1}{2}j\omega\mu_0 a\eta}{\frac{-2}{Y_e}+\eta\left(e^{-jka}-1\right)}H_y^i \approx \frac{\frac{1}{2}j\omega\mu_0 a\eta}{\frac{-2}{Y_e}-jka\eta}H_y^i. \tag{10}$$

With these, the electric field difference and effective magnetic current $\mathbf{M}'_{eff}$ produced by $\mathbf{J}_o$ is defined and calculated as

$$\begin{aligned}\mathbf{M}'_{eff} &\overset{\text{def}}{=} \left(\mathbf{E}_o^+ - \mathbf{E}_o^-\right)\times\hat{\mathbf{z}}\\ &= \left[\left(E_{ox}^{s+}+E_{ox}^{s-}e^{-jka}\right)-\left(E_{ox}^{s-}+E_{ox}^{s+}e^{-jka}\right)\right]\hat{\mathbf{x}}\times\hat{\mathbf{z}}\\ &\approx 2jkaE_{ox}^{s-}\hat{\mathbf{y}},\end{aligned} \tag{11}$$

where $\mathbf{E}_o^{\pm}$ are the total scattered electric fields at $z=\pm a/2$ respectively. They are equal in amplitude but out of phase. In addition, The effective magnetic current caused by the vacuum within the region between $z=-a/2$ and $z=a/2$ is

$$\mathbf{M}''_{eff} \overset{\text{def}}{=} \Delta\mathbf{E}^i\times-\hat{\mathbf{z}} \approx j\omega\mu_0 a H_y^i\hat{\mathbf{y}}. \tag{12}$$

The total magnetic fields at $z=-a/2-\delta$ and $z=a/2+\delta$, which can be shown to be equal, are

$$\mathbf{H}_t = \left(H_y^i - \frac{jka}{\eta}E_{ox}^{s-}\right)\hat{\mathbf{y}}, \tag{13}$$

with δ being a positive infinitesimal number.

According to definition, the effective magnetic surface impedance of the slab, which consists of the two electric metasurfaces as well as the vacuum between them, is found as

$$Z_{eff}^m = \frac{\mathbf{M}'_{eff}+\mathbf{M}''_{eff}}{\mathbf{H}_t} \approx \frac{j\omega\mu_0 a\frac{2}{Y_e}}{\frac{2}{Y_e}+\omega\mu_0 a\left(-\frac{1}{2}ka+j\right)}. \tag{14}$$

As can be seen, the separation distance a between the two electric metasurfaces gives rise to the effective magnetic surface impedance. When $a=0$, $Z_m=0$.

2.2. Effective Surface Electric Admittance

The incident electric field $\mathbf{E}^i$ excites the even mode surface electric current $\mathbf{J}_e$ as shown in Fig. 1(c). The scattered EM fields by $\mathbf{J}_e$ can be obtained in a similar way. The total electric field acting on the metasurfaces at $z=\pm a/2$ is found as

$$\mathbf{E}_t = \left(E_x^i + E_{ex}^{s-} + E_{ex}^{s+}e^{-jka}\right)\hat{\mathbf{x}}, \tag{15}$$

where $E_{ex}^{s-} = E_{ex}^{s+}$ is produced by the even mode current $\mathbf{J}_e^-$ and $\mathbf{J}_e^+$ respectively. $\mathbf{E}_t$ induces the surface electric current

$$\mathbf{J}_e^{\pm} = \frac{-2E_{ex}^{s-}}{\eta}\hat{\mathbf{x}}. \tag{16}$$

Using the surface electric impedance definition as above, we obtain

$$E_{ex}^{s-} = \frac{-E_x^i}{\dfrac{2}{Y_e\eta} + 1 + e^{-jka}}. \tag{17}$$

With it, the effective electric current produced by $\mathbf{J}_e$ is

$$\mathbf{J}'_{eff} \stackrel{\text{def}}{=} \hat{\mathbf{z}} \times \left(\mathbf{H}_e^+ - \mathbf{H}_e^-\right) = \frac{-2E_{ex}^{s-}}{\eta}\left(1 + e^{-jka}\right)\hat{\mathbf{x}}, \tag{18}$$

where $\mathbf{H}_e^{\pm}$ are the total scattered magnetic field at $z = \pm(a/2 + \delta)$, respectively, and δ is a positive infinitesimal number.

In addition, the incident E_x^i also introduces difference of the incident magnetic fields at $z = \pm a/2$. According to Ampere's law

$$\oint_L \mathbf{H}^i \cdot \mathbf{dl} = j\omega\epsilon_0 \int_S \mathbf{E}^i \cdot \mathbf{ds}, \tag{19}$$

we get

$$H_y^{i-}\hat{\mathbf{y}} \cdot \mathrm{d}l\hat{\mathbf{y}} + H_y^{i+}\hat{\mathbf{y}} \cdot -\mathrm{d}l\hat{\mathbf{y}} = j\omega\epsilon_0 \mathrm{d}l \int E_x^i e^{-jkz}\hat{\mathbf{x}} \cdot \mathrm{d}z\hat{\mathbf{x}}, \tag{20}$$

where $H_y^{i\pm}$ are the incident magnetic field complex amplitudes at $z = \pm a/2$ respectively. Eq. (20) can be simplified as

$$\Delta\mathbf{H}^i = \left(H_y^{i-} - H_y^{i+}\right)\hat{\mathbf{y}} \approx j\omega\epsilon_0 a E_x^i \hat{\mathbf{y}}. \tag{21}$$

The effective electric current (i.e., displacement current) produced by the vacuum between the two metasurfaces can be defined and calculated as

$$\mathbf{J}''_{eff} \stackrel{\text{def}}{=} -\hat{\mathbf{z}} \times \Delta\mathbf{H}^i = j\omega\epsilon_0 a E_x^i \hat{\mathbf{x}}, \tag{22}$$

With Eqs. (15), (18) and (22), the effective surface electric admittance due to the two electric metasurfaces is obtained as

$$Y_{eff}^e = \frac{\mathbf{J}'_{eff} + \mathbf{J}''_{eff}}{\mathbf{E}_t} \approx \left[2 + \frac{(ka)^2}{2}\right] Y_e + j\omega\epsilon_0 a. \tag{23}$$

As can be seen, when the separation distance $a = 0$, the effective surface electric admittance is just the parallel admittance of the two electric metasurfaces.

3. SIMULATION VERIFICATION

To verify the derived formulas of the effective surface impedances, we modeled the two parallel electric metasurface illustrated in the inset of Fig. 2(a) using a commercial EM software based on Finite Element Method. Both metasurfaces have the electric surface admittance $Y_e = 1/(80 + j100)$, and they are separated by 3 mm. The effective surface impedances are retrieved by the formulas

$$Y^{\mathrm{e}} = (2/\eta)\left[1 - (R+T)\right]/\left[1 + (R+T)\right], \tag{24a}$$

$$Z^{\mathrm{m}} = (2\eta)\left[1 + (R-T)\right]/\left[1 - (R-T)\right], \tag{24b}$$

where $\eta = 377\Omega$, R and T are the reflection and transmission coefficients of the model for normal incidence with the reference planes located at the two metasurfaces [24]. The simulation and theoretical results are given in Fig. 2. It can be seen that good agreements are achieved, which validates the derived formulas. In addition, the theory for the effective surface impedances can be generalized to two electric metasurfaces separated by any distance if the approximation $e^{-jka} \approx 1 - jka$ is not taken. Hence, two parallel electric metasurfaces with any distance in between can provide both effective electric and magnetic surface impedances.

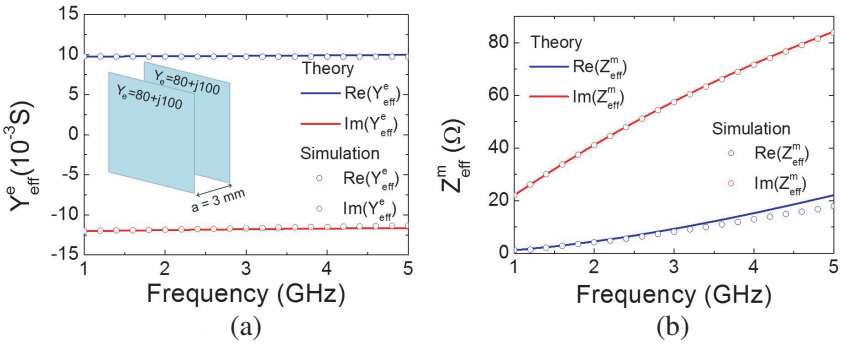

Figure 2. Simulation verification of the derived formulas for the effective (a) surface electric admittance and (b) surface magnetic impedance of the two parallel electric metasurfaces.

4. APPLICATION IN HIGH EFFICIENCY POLARIZATION CONVERSION

In regard of applications, the advantage of using parallel planar electric metasurfaces to produce effective surface magnetic impedance is the simplified structure and fabrication procedure compared to metallic loop structures [23, 24]. The loop structure requires vias in realization, which are too complicated to realize at very high frequencies, such as optical frequencies. In these frequency spectrum, simple and planar structures are more compliable with present fabrication technologies [25, 34, 35]. Hence, the proposed synthesis method in this paper is more compatible with practical fabrication capabilities. We will show that not only the effective magnetic surface impedance can be realized by the proposed method, but also the effective electric surface impedance, which is also important in metasurface designs, can be designed and adjusted simultaneously, with no influence on the effective magnetic surface impedance, by adding a middle layer electric surface. In other words, the effective surface electric and magnetic impedances can be designed individually and easily using the proposed synthesis method. To demonstrate this point, as an example, we designed a linear to circular polarization converter using only multiple planar electric metasurfaces, which can completely convert the linearly polarized incident waves to the circularly polarized transmitted waves with no energy reflection. High energy transmission is desired to improve signal noise ratio in practice, which requires both surface magnetic and electric impedance in synthesis. With only single layer electric impedance surface, as in [25, 24, 35], the incident energy will be partly reflected, leading to lower transmission efficiency.

The effective surface impedance of this polarization converter is calculated to be $\mathbf{Y}^e = \begin{pmatrix} j0.0022 & 0 \\ 0 & -j0.0022 \end{pmatrix}$ and $\mathbf{Z}^m = \begin{pmatrix} -j312 & 0 \\ 0 & j312 \end{pmatrix}$. Fig. 3(a) illustrates the unit cell structure to implement the required anisotropic surface impedance. It consists of three layers of electric metasurfaces; each one only provides the surface electric admittance. The metasurfaces on the top and bottom layers are identical. They provide the effective surface magnetic and electric impedances. As known from Eqs. (14) and (23), when the thickness parameter a is fixed, the effective surface impedance Z^m_{eff} and Y^e_{eff} are only determined by the surface electric admittance Y^e of each physical metasurface layer. Hence, after we optimize the Y_e to obtain the required Z^m_{eff} produced by the top and bottom layers, Y^e_{eff} can not be changed any more. To obtain the required Y^e_{eff}, we insert another metasurface as the middle layer as shown. The inserted layer produces the electric surface admittance that is parallel with that produced by the top and bottom layers. They contribute to the total effective surface electric admittance required in design. Moreover, it can be shown that the insertion of the middle layer does not change the effective surface magnetic impedance, so that these two types of surface impedance can be designed individually.

The unit cell has the dimension of 10 mm by 10 mm by 1.6 mm. The metallic wire width is 0.3 mm, and its conductivity is $5.8e+07$ S/m. The distance between the two polarities of the capacitor gap is 0.3 mm. The width of the capacitors in the x direction on the top and bottom layers is 0.8 mm, and that on the center layer is 1.9 mm. The width of the capacitors in the y direction on the top and bottom layers is 1.22 mm, and that on the middle layer is 1.09 mm. The relative dielectric constant of

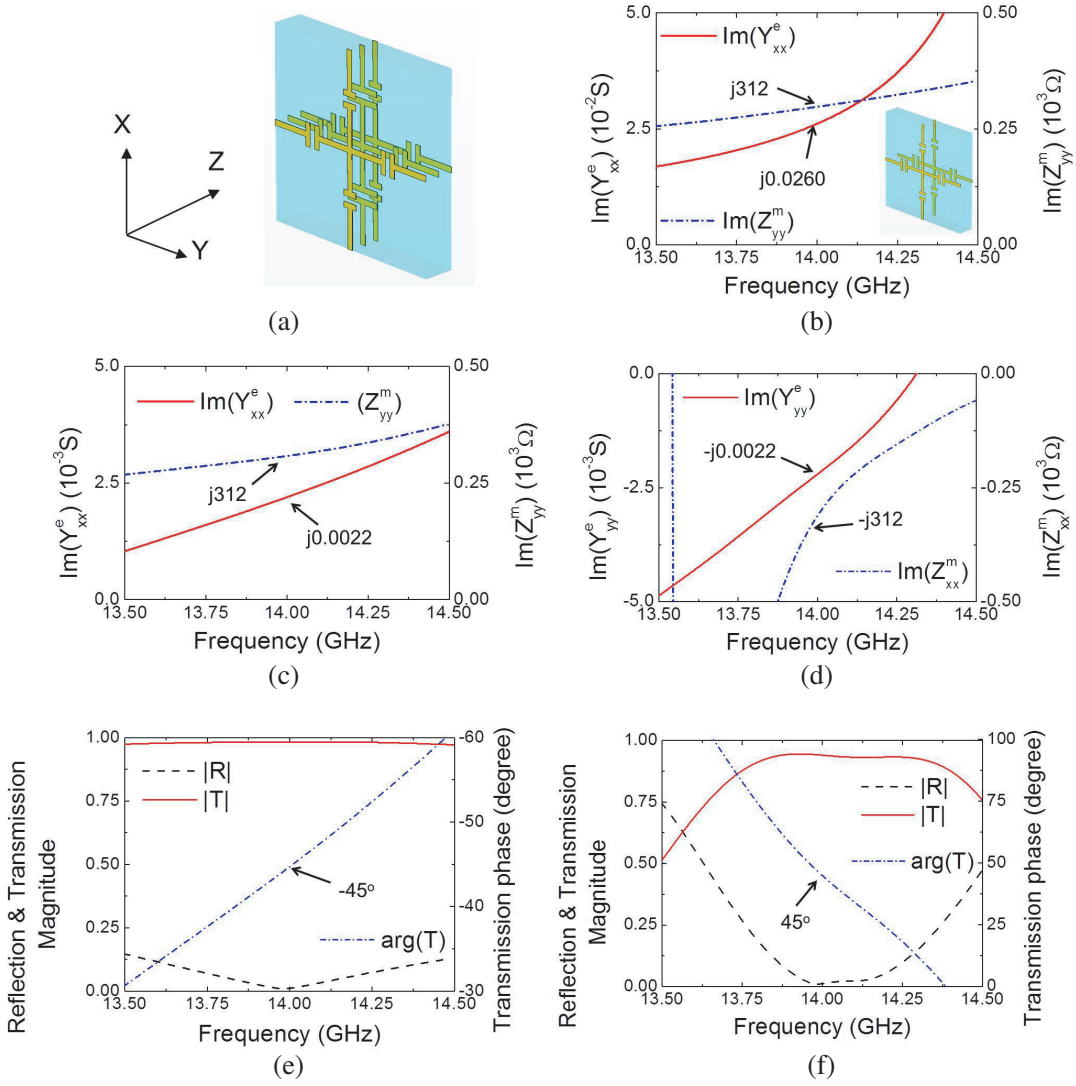

Figure 3. (a) Unit cell of the planar linear to circular polarization converter. (b) Parallel electric metasurfaces to produce effective surface electric and magnetic impedances. (c), (d) Realized anisotropic surface impedance tensors for polarization conversion. Nearly unity transmission magnitude and null reflection is achieved at 14 GHz, with (e) $-45°$ and (f) $45°$ transmission phase for two orthogonally polarized incident waves, respectively.

the substrate is 2.2, loss tangent 0.002.

Figure 3(b) shows the effective surface electric and magnetic impedances generated only by the top and bottom layers. The real parts of the retrieved surface impedance are not shown because of their small values. Note that there is no the middle layer as shown in the inset figure. The effective surface magnetic impedance for the y component of magnetic field is $j312$ at 14 GHz, which is equal to the required parameters given above. The effective surface electric admittance is, however, $j0.0260$, which is different from the required value. Hence, a middle electric metasurface is inserted to compensate this mis-match. As shown in Fig. 3(c), the effective surface electric admittance is now $j0.0022$, which is equal to the require value. In addition, adding the middle layer doesn't change the effective surface magnetic impedance, as can be seen from the equality between the curves of $\mathrm{Im}(Z^m_{yy})$ in Figs. 3(b) and (c). This is because the odd mode of incident electric field, that excites the circulating electric current as illustrated in Fig. 1(b), is zero at the middle layer. By the same procedure, the required effective is obtained for the

orthogonally polarized incident wave, as shown in Fig. 3(d). Figs. 3(e) and (f) show the transmission and reflection of the unit cell for two normal incident waves with mutually orthogonal polarizations. As seen, at 14 GHz, nearly unity transmission magnitude and null reflection is achieved, and transmission phase is $\pm 45^\circ$ for these orthogonally polarized waves. Therefore, this device can transform a linearly polarized waves to circularly polarized wave in transmission with high energy efficiency.

5. CONCLUSION

In summary, we have rigorously proved that effective surface magnetic impedance can be implemented by parallel planar metasurfaces with identical surface electric admittances. The effective magnetic current is excited by the odd mode of the incident electric field because of the time-varying magnetic field, whereas the effective electric current is due to the even mode of the incident electric field. The displacement current and magnetic field between the planar metasurface layers also contribute to the effective surface impedance. A polarization converter composed of three layers of planar electric metasurfaces is presented, which verifies the theoretical prediction. Under oblique incidence, even and odd modes still exist in the incident electric field, so that effective surface magnetic and electric impedance can still be obtained with planar electric metasurfaces in a similar way. In addition, the proposed idea may be generalized to achieve surface magnetic impedance tensors using parallel metasurfaces with tenor electric surface impedance. Effective chiral effect can also be obtained if parallel metasurfaces with different surface electric impedances are employed. Conventionally, effective surface magnetic impedance had to be realized using metallic loop structures, which requires the use of vias or non-planar fabrication process. The proposed planar structure and synthesis method effectively simplifies metasurface designs and fabrications.

ACKNOWLEDGMENT

This work is supported by National Science Foundation of China (NSFC) (61571216, 61301017), The Project funded by the Priority Academic Development of Jiangsu Higher Education Institutions (PAAD) and The Fundamental Research Funds for the Central Universities (021014380051).

REFERENCES

1. Glybovski, S. B., S. A. Tretyakov, P. A. Belov, Y. S. Kivshar, and C. R. Simovski, "Metasurfaces: From microwaves to visible," *Physics Reports*, Vol. 634, No. 1, 72, 2016.
2. Kuester, E. F., M. A. Mohamed, M. Piket-May, and C. L. Holloway, "Averaged transition conditions for electromagnetic fields at a metafilm," *IEEE Trans. Antennas Propagat.*, Vol. 51, No. 10, 2641–2651, Oct. 2003.
3. Holloway, C. L., M. A. Mohamed, E. F. Kuester, and A. Dienstfrey, "Reflection and transmission properties of a metafilm: With an application to a controllable surface composed of resonant particles," *IEEE Trans. Electomag. Compat.*, Vol. 47, No. 4, 853–865, Nov. 2005.
4. Yu, N., P. Genevet, M. A. Kats, F. Aieta, J.-P. Tetienne, F. Capasso, and Z. Gaburro, "Light propagation with phase discontinuities: Generalized laws of reflection and refraction," *Science*, Vol. 334, No. 6054, 333–337, 2011.
5. Holloway, C. L., E. F. Kuester, J. A. Gordon, J. O'Hara, J. Booth, and D. R. Smith, "An overview of the theory and applications of metasurfaces: The two-dimensional equivalents of metamaterials," *IEEE Antennas and Propagation Magazine*, Vol. 54, No. 2, 10–35, Apr. 2012.
6. Niemi, T., A. O. Karilainen, and S. A. Tretyakov, "Synthesis of polarization transformers," *IEEE Trans. Antennas Propagat.*, Vol. 61, No. 6, 3102–3111, Jun. 2013.
7. Selvanayagam, M. and G. V. Eleftheriades, "Discontinuous electromagnetic fields using orthogonal electric and magnetic currents for wavefront manipulation," *Opt. Express*, Vol. 21, No. 12, 14409–14429, Jun. 17, 2013.
8. Kildishev, A. V., A. Boltasseva, and V. M. Shalaev, "Planar photonics with metasurfaces," *Science*, Vol. 339, No. 6125, 2013.

9. Memarzadeh, B. and H. Mosallaei, "Array of planar plasmonic scatterers functioning as light concentrator," *Opt. Lett.*, Vol. 36, No. 13, 2569–2571, 2011.
10. Papakostas, A., A. Potts, D. M. Bagnall, S. L. Prosvirnin, H. J. Coles, and N. I. Zheludev, "Optical manifestations of planar chirality," *Phys. Rev. Lett.*, Vol. 90, 107404, Mar. 2003.
11. Huang, L., X. Chen, H. Müehlenbernd, H. Zhang, S. Chen, B. Bai, Q. Tan, G. Jin, K.-W. Cheah, C.-W. Qiu, J. Li, T. Zentgraf, and S. Zhang, "Three-dimensional optical holography using a plasmonic metasurface," *Nat. Commun.*, 4, Nov. 2013.
12. Shitrit, N., I. Yulevich, E. Maguid, D. Ozeri, D. Veksler, V. Kleiner, and E. Hasman, "Spin-optical metamaterial route to spin-controlled photonics," *Science*, Vol. 340, No. 6133, 724–726, May 10, 2013.
13. Niv, A., G. Biener, V. Kleiner, and E. Hasman, "Spiral phase elements obtained by use of discrete space-variant subwavelength gratings," *Opt. Commun.*, Vol. 251, No. 4–6, 306–314, 2005.
14. Genevet, P., N. Yu, F. Aieta, J. Lin, M. A. Kats, R. Blanchard, M. O. Scully, Z. Gaburro, and F. Capasso, "Ultra-thin plasmonic optical vortex plate based on phase discontinuities," *Appl. Phys. Lett.*, Vol. 100, No. 1, 013101, Jan. 2012.
15. Shu, W., D. Song, Z. Tang, H. Luo, Y. Ke, X. Lv, S. Wen, and D. Fan, "Generation of optical beams with desirable orbital angular momenta by transformation media," *Phys. Rev. A*, Vol. 85, 063840, Jun. 2012.
16. Chen, M. L. N., L. J. Jiang, and W. E. I. Sha, "Ultrathin complementary metasurface for orbital angular momentum generation at microwave frequencies," *IEEE Trans. Antennas Propagat.*, Vol. 65, No. 1, 396–400, Jan. 2017.
17. Ding, X., F. Monticone, K. Zhang, L. Zhang, D. Gao, S. N. Burokur, A. de Lustrac, Q. Wu, C.-W. Qiu, and A. Alu, "Ultrathin pancharatnamberry metasurface with maximal cross-polarization efficiency," *Advanced Materials*, Vol. 27, No. 7, 1195–1200, Feb. 2015.
18. Yu, N., F. Aieta, P. Genevet, M. A. Kats, Z. Gaburro, and F. Capasso, "A broadband, background-free quarter-wave plate based on plasmonic metasurfaces," *Nano Lett.*, Vol. 12, No. 12, 6328–6333, 2012, PMID: 23130979.
19. Hasman, E., V. Kleiner, G. Biener, and A. Niv, "Polarization dependent focusing lens by use of quantized pancharatnam-berry phase diffractive optics," *Appl. Phys. Lett.*, Vol. 82, No. 3, 328–330, 2003.
20. Chen, X., L. Huang, H. Mühlenbernd, G. Li, B. Bai, Q. Tan, G. Jin, C.-W. Qiu, S. Zhang, and T. Zentgraf, "Dual-polarity plasmonic metalens for visible light," *Nat. Commun.*, Vol. 3, 1198, Nov. 2012.
21. Aieta, F., P. Genevet, M. A. Kats, N. Yu, R. Blanchard, Z. Gaburro, and F. Capasso, "Aberration-free ultrathin at lenses and axicons at telecom wavelengths based on plasmonic metasurfaces," *Nano Lett.*, Vol. 12, No. 9, 4932–4936, 2012, PMID: 22894542.
22. Pors, A., M. G. Nielsen, R. L. Eriksen, and S. I. Bozhevolnyi, "Broadband focusing at mirrors based on plasmonic gradient metasurfaces," *Nano Lett.*, Vol. 13, No. 2, 829–834, 2013, PMID: 23343380.
23. Pfeiffer, C. and A. Grbic, "Metamaterial huygens surfaces: Tailoring wave fronts with re ectionless sheets," *Phys. Rev. Lett.*, Vol. 110, 197401, 2013.
24. Zhu, B. O., K. Chen, N. Jia, L. Sun, J. Zhao, T. Jiang, and Y. Feng, "Dynamic control of electromagnetic wave propagation with the equivalent principle inspired tunable metasurface," *Sci. Rep.*, 4, May 15, 2014.
25. Zhao, Y. and A. Alù, "Manipulating light polarization with ultrathin plasmonic metasurfaces," *Phys. Rev. B*, Vol. 84, 205428, Nov. 2011.
26. Zhang, X., Z. Tian, W. Yue, J. Gu, S. Zhang, J. Han, and W. Zhang, "Broadband terahertz wave de ection based on c-shape complex metamaterials with phase discontinuities," *Advanced Materials*, Vol. 25, No. 33, 4567–4572, 2013.
27. Kang, M., T. Feng, H.-T. Wang, and J. Li, "Wave front engineering from an array of thin aperture antennas," *Opt. Express*, Vol. 20, No. 14, 15882–15890, Jul. 2012.

28. Epstein, A. and G. V. Eleftheriades, "Passive lossless huygens metasurfaces for conversion of arbitrary source field to directive radiation," *IEEE Trans. Antennas Propagat.*, Vol. 62, No. 11, 5680–5695, Nov. 2014.
29. Kim, M., H. Wong, M. Alex and G. V. Eleftheriades, "Optical huygens' metasurfaces with independent control of the magnitude and phase of the local reflection coefficients," *Phys. Rev. X*, Vol. 4, 041042, Dec. 2014.
30. Zhao, Y., M. A. Belkin, and A. Alù, "Twisted optical metamaterials for planarized ultrathin broadband circular polarizers," *Nat. Commun.*, Vol. 3, 870, May 2012.
31. Monticone, F., N. M. Estakhri, and A. Alù, "Full control of nanoscale optical transmission with a composite metascreen," *Phys. Rev. Lett.*, Vol. 110, 203903, 2013.
32. Pfeiffer, C., N. K. Emani, A. M. Shaltout, A. Boltasseva, V. M. Shalaev, and A. Grbic, "Efficient light bending with isotropic metamaterial huygens surfaces," *Nano Lett.*, Vol. 14, No. 5, 2491–2497, 2014, PMID: 24689341.
33. Pfeiffer, C. and A. Grbic, "Bianisotropic metasurfaces for optimal polarization control: Analysis and synthesis," *Phys. Rev. Applied*, Vol. 2, 044011, Oct. 2014.
34. Strikwerda, A. C., K. Fan, H. Tao, D. V. Pilon, X. Zhang, and R. D. Averitt, "Comparison of birefringent electric split-ring resonator and meanderline structures as quarter-wave plates at terahertz frequencies," *Opt. Express*, Vol. 17, No. 1, 136–149, Jan. 2009.
35. Euler, M., V. Fusco, R. Cahill, and R. Dickie, "325 GHz single layer sub-millimeter wave fss based split slot ring linear to circular polarization convertor," *IEEE Trans. Antennas Propagat.*, Vol. 58, No. 7, 2457–2459, Jul. 2010.